

The Schmidt Law at High Molecular Densities

Shinya KOMUGI, Yoshiaki SOFUE, Hiroyuki NAKANISHI*, Sachiko ONODERA
and

Fumi EGUSA

Institute of Astronomy, University of Tokyo, 2-21-1 Osawa, Mitaka-shi, Tokyo, 181-8588, Japan

**Nobeyama Radio Observatory, Minamisaku, Nagano, 384-1305, Japan*

skomugi@ioa.s.u-tokyo.ac.jp

(Received ; accepted)

Abstract

We have combined H α and recent high resolution ^{12}CO (J=1-0) data to consider the quantitative relation between gas mass and star formation rate, or the so-called Schmidt law in nearby spiral galaxies at regions of high molecular density. The relation between gas quantity and star formation rate has not been previously studied for high density regions, but using high resolution CO data obtained at the NMA(Nobeyama Millimeter Array), we have found that the Schmidt law is valid at densities as high as $10^3\text{M}_\odot\text{pc}^{-2}$ for the sample spiral galaxies, which is an order of magnitude denser than what has been known to be the maximum density at which the empirical law holds for non-starburst galaxies. Furthermore, we obtain a Schmidt law index of $N = 1.33 \pm 0.09$ and roughly constant star formation efficiency over the entire disk, even within the several hundred parsecs of the nucleus. These results imply that the physics of star formation does not change in the central regions of spiral galaxies. Comparisons with starburst galaxies are also given. We find a possible discontinuity in the Schmidt law between normal and starburst galaxies.

Key words: galaxies:ISM — galaxies:spiral — ISM:molecules — stars:formation

1. Introduction

The global, disk-averaged star formation rate Σ_{SFR} and gas density Σ_{SMD} in nearby galaxies are known to be well correlated, producing a simple power law called the Schmidt law; $\Sigma_{\text{SFR}} \propto \Sigma_{\text{SMD}}^N$ (Schmidt 1959). The determination of the index N has been extensively studied, producing values between 1 and 2. However, the density range at which this law holds for normal galaxies has not been studied as much. The lower density cutoff for the Schmidt law has been argued by Kennicutt (1989) based on gravitational instability, giving a critical gas density of 5 to 10 $\text{M}_\odot\text{pc}^{-2}$ where star formation is strongly suppressed below this limit. On

the other hand, there has been only marginal success for the observational consideration of the Schmidt law at higher densities. This is primarily due to the limit in spatial resolution of CO observations, where the $^{12}\text{CO}(J=1-0)$ emission at $\lambda=2.6\text{mm}$ is used as a tracer of molecular gas.

High molecular density regions are spatially small in general, owing to the molecular cloud's patchy structure and central condensation (Sakamoto et al. 1999). Therefore, it is essential to make CO observations with smaller beam sizes (higher resolution). Rownd & Young (1999) have shown that the Schmidt law holds better when sampled within galaxies, using 45 arcsecond resolution data at the center of over 100 nearby galaxies (see figure 11 in Rownd & Young (1999)). However, the densest gas in galaxies is normally confined to within a few hundred parsecs of the nucleus (e.g., Sakamoto et al. (1999), Sofue et al. (2003a)). Therefore, 45 arcsecond resolution, which corresponds to kpc scales in nearby galaxies, is too large to consider the validity of the Schmidt law at the highest densities. Kennicutt (1998) has shown that the Schmidt law holds at higher densities if we include a sample of IR luminous starburst galaxies with $L_{\text{FIR}} \sim 10^8 - 10^{10}L_{\odot}$ to $L_{\text{FIR}} \leq 10^{12}L_{\odot}$ at high molecular densities. Including this sample has extended the Schmidt law up to an unchallenged value of $\Sigma_{\text{SMD}} \sim 10^5 M_{\odot} \text{pc}^{-2}$ (see figure 6 in Kennicutt (1998)). However, IR luminous starbursts represent special physical conditions which display a systematic difference from normal spirals, and including this sample in considering the validity of the Schmidt law may lead us to a misunderstanding of the physical properties which underly the poorly understood power law. Gao & Solomon (2004) have indeed found that the IR luminous galaxies with $L_{\text{IR}} \leq 10^{11}L_{\odot}$ do display a systematic difference from normal galaxies in view of the Schmidt law, in that the ratio of HCN to CO rises abruptly for IR luminous galaxies compared to normal galaxies. Exclusion of these IR luminous samples from Kennicutt(1998) and the consideration of only normal spirals reveal that the law is only valid up to $\sim 10^2 M_{\odot} \text{pc}^{-2}$. Other studies of the Schmidt law at high densities involve HCN (Gao & Solomon 2004) and higher transition emission such as $^{12}\text{CO}(J=2-1)$ as probes of hydrogen at higher densities, but the weakness of this emission and the difficulty in comparing Σ_{SMD} derived from these probes and others of lower density (such as $\text{CO}(J=1-0)$ and HI) has limited the consistent consideration of the Schmidt law's validity at a wide density range.

In order to approach to a more fundamental understanding of the relation between gas content and star formation, it is essential to know to what density the Schmidt law holds for normal galaxies, or whether the simple power-law formulation of the Schmidt law is valid at all. This will require that we use a consistent probe of the gas, at a wide density range.

In this study, we consider the validity of the Schmidt Law including densities above this limit by using recent high resolution single dish and interferometry observations. Section 2 provides information on CO and $\text{H}\alpha$ data, and the procedures for calculating Σ_{SMD} and Σ_{SFR} . In section 3 we show the result, and in section 4 we discuss the various uncertainties which relate to the Schmidt law, and the validity of the Schmidt law at high densities. Conclusions

Table 1. Basic properties of the sample galaxies

Galaxy	R.A.	Decl.	Type	D(Mpc)	i(degrees)	size (arcmin)
(1)	(2)	(3)	(4)	(5)	(6)	(7)
NGC2903	09 29 19.9	+21 43 19	SAB	6.3	60	11.2
NGC3593	11 11 59.2	+13 05 28	SA	5.5	67	4.9
NGC4041	11 59 38.7	+62 25 03	SA	22.7	18	2.9
NGC4192	12 11 15.4	+15 10 23	SAB	16.8	74	7.8
NGC4212	12 13 06.4	+14 10 45	SA	16.8	47	2.9
NGC4254	12 16 16.9	+14 41 46	SA	16.8	28	5.5
NGC4303	12 19 21.4	+04 44 58	SAB	16.8	25	6.2
NGC4321	12 20 23.2	+16 06 00	SAB	16.8	28	7.1
NGC4419	12 24 25.1	+15 19 28	SB	16.8	67	2.8
NGC4501	12 29 28.1	+14 41 50	SA	16.8	58	6.3
NGC4535	12 31 47.9	+08 28 25	SAB	16.8	43	6.6
NGC4536	12 31 53.5	+02 27 50	SAB	16.8	67	6.5
NGC4548	12 32 55.1	+14 46 20	SB	16.8	37	5.4
NGC4569	12 34 18.7	+13 26 18	SAB	16.8	63	8.3
NGC4579	12 35 12.6	+12 05 40	SAB	16.8	37	5.4
NGC4654	12 41 25.7	+13 23 58	SAB	16.8	52	4.4
NGC4689	12 45 15.3	+14 02 13	SA	16.8	30	4.1
NGC4736	12 48 32.4	+41 23 28	SA	4.3	35	11
NGC4826	12 54 16.9	+21 57 18	SA	4.1	57	9.3
NGC5005	13 08 37.6	+37 19 25	SAB	21.3	62	4.8
NGC5194	13 27 46.9	+47 27 16	SA pec	7.7	20	10.5
NGC5248	13 35 02.4	+09 08 23	SAB	22.7	42	6.3
NGC6946	20 33 48.8	+59 58 50	SAB	5.5	30	13.2

NOTES-Units of right ascension are hours, minutes, and seconds, and units of declination are degrees, arcminutes, and arcseconds. Col.(1):Galaxy name. Col.(2)(3):Galaxy coordinates(epoch 1950). Col.(4):Hubble Type, taken from RC2. Col.(5): Distance to the galaxy, adopted from Ho et al. (1997). Col.(6):Inclination angle, given in Young et al. (1995). Col.(7):Projected diameter, taken from Rownd & Young (1999).

will be given in section 5.

Table 2. CO and H α reference

	Region	CO	H α
Global average	E	(1)	(1)
central 45 arcsec	D	(2)	(2)
central 16 arcsec	C	(3)	(4)
central 6 arcsec	B	(5)	(4)
central 3 arcsec	A	(6),(7)	(8)

Notes- Reference(1):Young et al. (1996) (2):Rownd & Young (1999) (3):Nishiyama & Nakai (2001) (4):Koopmann et al. (2001) (5)Helfer et al. (2003) (6):Sakamoto et al. (1999) (7):Sofue et al. (2003a) (8):Ho et al. (1997) Data for the central 6 arcseconds were retrieved only for NGC4303, NGC4321, NGC4535, NGC4548 and NGC4569. Data for the central 16 arcseconds were retrieved only for NGC4254, NGC4303, NGC4501, NGC4535 and NGC4569. Global average, central 45 and 3 arcsecond data were retrieved for all of the sample galaxies. Data from (2), (4), (6) and (7) were traced from radial profiles given in the reference. For galaxies which overlapped in (6) and (7), data from Sofue et al. (2003a) were used.

2. Data

We have made high resolution (typically 3 arcsecond) $^{12}\text{CO}(J=1-0)$ observations of galaxies in the Virgo Cluster, with the NMA(Nobeyama Millimeter Array). Observational parameters and data are presented in Sofue et al. (2003a). Using the obtained data and other high resolution CO data obtained mainly at NRO (Nobeyama Radio Observatory), and further combining it with low resolution single dish observations in other studies to account for intermediate gas density regions, we have studied the validity of the Schmidt law at a wide density range within 23 spiral galaxies. Fundamental parameters of the sample galaxies are listed in table 1.

2.1. Sample selection

Rownd & Young (1999) have found that the Schmidt law holds better when data are sampled locally within galaxies, with smaller beam size. However, their study used CO and H α data at 45 arcsecond resolution, too large to consider high density regions which are typically small in size. In order to consider the Schmidt law for a wide range of gas density, we have chosen galaxies which have been observed in several beam sizes. Twenty three spiral galaxies were chosen, 14 of which are members of the Virgo Cluster. All are spirals, SA, SAB, or SB in morphology. Most samples have 3 data points corresponding to different beam sizes, expressing different density ranges. Some galaxies have been observed in more beam sizes. NGC4254, NGC4321, NGC4501, NGC4548, and NGC4579 have 4 data points, and NGC4303, NGC4535, and NGC4569 have 5 data points. The inclination angle i (degrees), total blue magnitude B_{tot} , and peak $^{12}\text{CO}(J=1-0)$ line antenna temperature T_A^* (mK) are in the range $18 \leq i \leq 74$, $8.99 \leq B_{\text{tot}} \leq 12.08$, and $21 \leq T_A^* \leq 312$, respectively.

2.2. CO data

CO and H α data used in this study are listed in table 2. Much of the interferometric data were obtained in the course of “Virgo High-resolution CO Survey”, a long-term project at Nobeyama Millimeter Array (Sofue et al. 2003a). We have combined data with different spatial resolutions, so that data with low resolution, which averages a large area within the galaxy would give low density values, whereas high resolution data at galactic centers would give high molecular densities. Molecular gas densities in the literature were recalculated using a conversion factor of $X_{\text{CO}} = 2.0 \times 10^{20} \text{ (cm}^{-2} \cdot \text{K}^{-1} \cdot \text{km}^{-1} \cdot \text{s)}$ and the formulation

$$\left[\frac{\Sigma_{\text{SMD}}}{\text{g} \cdot \text{cm}^{-2}} \right] = 2 \times \left[\frac{m_{\text{H}}}{\text{g}} \right] \times X_{\text{CO}} \left[\frac{I_{\text{CO}}}{\text{K} \cdot \text{km} \cdot \text{s}^{-1}} \right] \times 1.6 \quad (1)$$

where m_{H} and I_{CO} are the mass of a hydrogen atom, and CO intensity, respectively. X_{CO} is poorly understood for the sample galaxies, and the value we adopt is the mean value of those derived for our galaxy and other disk galaxies (e.g., Sanders et al. (1984), Bloemen et al. (1986), Solomon et al. (1987), Nakai & Kuno (1995)). The factor 1.6 accounts for mass of heavy elements. Gas densities for each of the regions within the galaxies were derived in the following manner:

1. The highest resolution data (~ 3 arcseconds, see table 2) was used to derive the gas mass at the central-most region. We call this region *A*
2. Then, the second-highest resolution data (6, 16 or 45 arcseconds, the highest for the individual galaxy for which we have retrieved data) which was also centered on the nucleus was used to derive the gas mass within the beam.
3. Gas mass derived from 1. was subtracted from that derived in 2. This would give the gas mass confined within the annulus corresponding to the difference in the area of the two beam sizes. We call this region in the annulus *B*.
4. The same procedures 1 through 3 were repeated for larger beam sizes, and then the surface gas densities were derived for each of the annuli. Each of the annuli are labeled *C*, *D*, and *E*, respectively, in the order of increasing beam size. Note that region *E* uses the global averaged value, and is not actually derived from a single beam.

This procedure divides the galaxy into several annuli, so that derived gas densities give radial dependent values. We present a schematic picture of the regions in figure 1.

2.3. H α data

The calculation of the star formation rate $\Sigma_{\text{SFR}} \text{ M}_{\odot} \text{pc}^{-2} \text{yr}^{-1}$ was conducted following Kennicutt (1998), using the H α luminosity emitted from ionized gas around young massive stars.

$$\left[\frac{\Sigma_{\text{SFR}}}{\text{M}_{\odot} \cdot \text{pc}^{-2} \cdot \text{yr}^{-1}} \right] = \left[\frac{L(\text{H}\alpha)}{1.26 \times 10^{41} \text{ erg} \cdot \text{s}^{-1}} \right] \times \left[\frac{S}{\text{pc}^2} \right]^{-1} \quad (2)$$

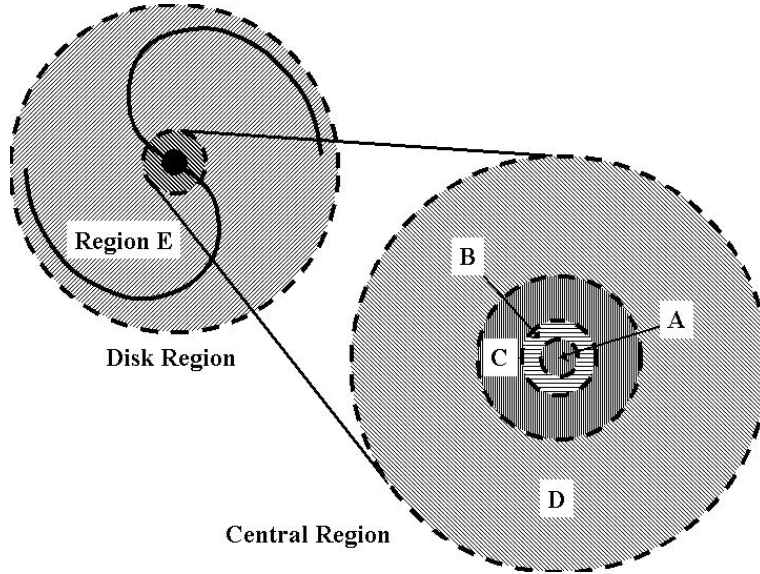


Fig. 1. Schematic picture of the regions A through E. The dotted lines indicate the edge of each of the regions. The regions are scaled using an arbitrary global diameter (edge of region E) of 5 arcminutes (the average for Virgo galaxies).

where S is the projected area of $H\alpha$ emission. Procedures as same as the CO data (1. through 4.) were applied to the $H\alpha$ data for the calculation of the Σ_{SFR} .

Galactic extinction has been corrected for all of the data. The original references adopt different extinction laws, and they were recalculated using the same form of $A(H\alpha) = 0.08(\csc|b| - 1)$ in magnitudes, where b is the Galactic latitude, where possible (regions A, D, and E). In the original references (see table 2), galactic extinction for regions B and C were corrected using Landolt standards or the standard extinction curve at Kitt Peak National Observatory or Cerro Tololo Inter-American Observatory. The references for regions B and C do not list the standard stars or the data before correction, so the corrected data from the original references were used without adopting the same extinction law. This will not make any significant changes, however, because the typical extinction due to the Galaxy is of order 0.01 to 0.1 mag; on the logarithmic scale, as we will use, this will be 0.004 to 0.04 on the ordinate. We therefore conclude, that Galactic extinction for the samples are satisfactorily corrected.

The reader should refer to the original references (see table 2) for details. Extinction within the sample galaxies (internal extinction) plays a role in the determination of the true $H\alpha$ luminosity at the central regions of galaxies, and the effects of extinction correction will be discussed in section 4.

3. Results

Figure 2 shows the Σ_{SMD} versus Σ_{SFR} on a logarithmic scale, for each of the regions in the sample galaxies. We see clearly that data plotted with smaller beam sizes account for

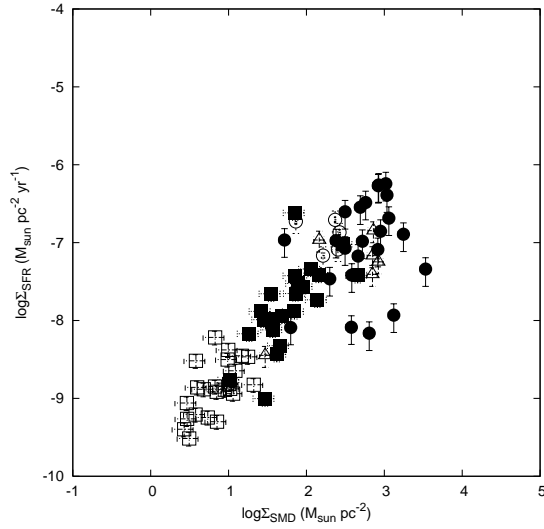


Fig. 2. The $\Sigma_{\text{SMD}} - \Sigma_{\text{SFR}}$ for all of the sample galaxies. Internal $\text{H}\alpha$ extinction has not been corrected for. Abscissa is $\log \Sigma_{\text{SMD}}$, ordinate $\log \Sigma_{\text{SFR}}$. Filled circles, triangles, open circles, filled squares, and open squares stand for regions A, B, C, D, and E, respectively. Horizontal error bars for filled circles lie within the symbol. Notice the several points in region A which are deviated from other plots.

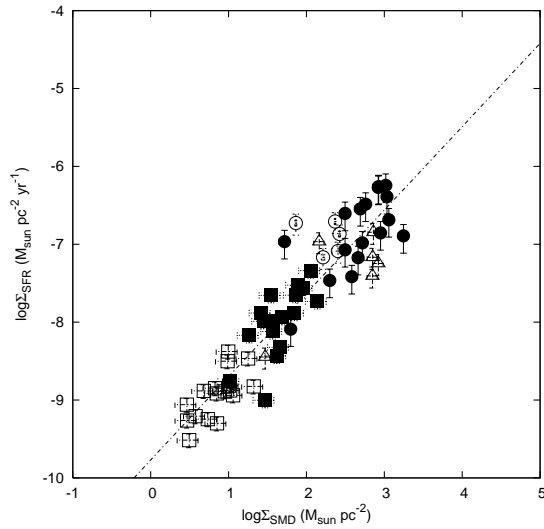


Fig. 3. The same figure as 2, with NGC2903, NGC3593, NGC4736, NGC4826, NGC5194, and NGC6946, excluded as mentioned in section 3. A best fit yields $N = 1.07 \pm 0.06$.

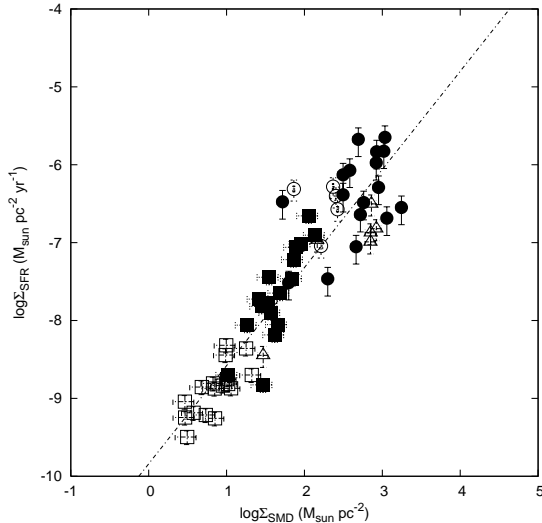


Fig. 4. The same figure as 3, corrected for $H\alpha$ extinction. A best fit yields $N = 1.33 \pm 0.08$.

the high density regime of the Schmidt law, extending to densities as high as $10^3 M_\odot \text{pc}^{-2}$. For the highest densities, data seems to be dispersed from the correlation. However, we find that galaxies which are dispersed from the correlation are those in the sample whose distances are closer to our Galaxy; namely, NGC3593, NGC4736, NGC4826, NGC6946 are only several Mpc away compared to 16.8 Mpc for most of the sample. The resolution of 3 arcseconds corresponds to under 100 pc for these galaxies. An investigation of the coordinates of the center of these galaxies in $H\alpha$ and CO will reveal that the CO intensity peaks are offset from $H\alpha$ centers, often by more than 3 arcseconds. We have excluded these galaxies in further analysis because there were possibility that the small beam of ~ 3 arcseconds do not include both the star forming region and its counterpart molecular cloud which is generally several $\times 10$ pc in size. In general, star forming regions do not coincide with the molecular clouds which give birth to them. This is seen in spirals arms, where the optical and the molecular spiral structure are offset. If only the molecular clouds are observed and not the star forming regions which are physically coupled to it, it will result in the gas density to show excess from the expected correlation. The data points for the 4 galaxies named above, seem to have this property. Although not significantly different from the other galaxies, NGC2903 and NGC5194 which have similar spatial resolution (under 100 pc) in Region A were also excluded. Moreover, it should be noted that $H\alpha$ luminosities of NGC4736, NGC4826, NGC5194 and NGC6946 were given only as lower limits in Ho et al. (1997). This leaves a subset of 17 galaxies in our sample. The same figure with these galaxies excluded are shown in figure 3. A tighter correlation can be seen through the gas density range. Figure 3 clearly shows that high density regions A, B, and C, and the lower density regions D and E, can be fitted with the same line. A least squares fit to figure 3 yields a Schmidt law index N of 1.14 ± 0.08 , allowing for errors in both of the axes.

4. Discussion

4.1. Error estimation

(1) Derivation of Σ_{SMD}

In general, we refer to gas mass as the total of both molecular and atomic mass. However, the legitimacy of using either or both of the hydrogen gas is not well known. While Kennicutt (1989) found that total gas density correlates better with the star formation rate, others such as Gao & Solomon (2004) believe that denser (hence, H_2 rather than HI) gas correlates better with the star formation rate. Boissier et al. (2003) find that total and molecular gas both correlate well with Σ_{SFR} , but the tight correlation seen in using the total gas is driven by the correlation of molecular gas with the star formation rate. The recent trend seems to be in favor of using only molecular gas, but it is still controversial. We use only molecular gas in our study, on the following grounds; (1) massive star formation presumably occurs in molecular clouds cores, where HI is less abundant. On the standpoint that star formation is a two step process where H_2 clouds are first formed from HI, and stars are then formed from H_2 , we conclude that H_2 should be a more direct tracer of the star formation rate. (2) We are interested in high density regions of galaxies, and have used galactic centers. These regions are known to be HI deficient, so even if HI plays a role in star formation, its mass should be negligible.

Another uncertainty resides in the CO to H_2 conversion factor X_{CO} . The constant value of $X_{\text{CO}} = 2.0 \times 10^{20}$ is highly questionable. However, the conversion factor for each of the sample galaxies is not known, and moreover it's variation within those galaxies are potentially difficult to know; we have used the average value of our galaxy and galaxies with known X_{CO} uniformly for all of the data for the sake of simplicity. Boissier et al. (2003) have found that by using metallicity dependent X_{CO} , Σ_{SMD} should change typically by a factor of 2 to 3 in the central regions compared to disk regions of nearby spirals, in the sense of decreasing gas mass. This, however, does not make disastrous changes compared to using a constant conversion factor, because factors of 2 to 3 makes little difference to the positions in which data are plotted on the $\log \Sigma_{\text{SMD}} - \log \Sigma_{\text{SFR}}$ scale. Again, we adopt the constant X_{CO} for the sake of uniformity and simplicity.

The highest resolution measurements use interferometers, which has the “missing flux” problem. Spatially extended sources can not be detected, which has the effect of underestimating the surface density. Figure 3 indicates that compared to region D with 45 arcsecond resolution, region A and B with the interferometric observations are typically an order of magnitude higher in Σ_{SMD} . Even compared to region C with 16 arcsecond resolution, region A is higher typically by a factor of about 3. This indicates that the missing flux has no significant effect on Σ_{SMD} .

The horizontal error bars in figure 3 do not include the uncertainties given above. They

are typically 15 to 30%, and are mainly due to errors in flux calibration, given in the original references.

(2)H α extinction

The H α emission lines are subject to extinction within the target galaxies, and we must also account for this in the analysis. A global, uniform extinction correction of ~ 1 mag. is suggested by Kennicutt & Kent (1983), but this is an oversimplification, because central regions of galaxies are generally thought to be subject to larger extinction than disk regions. Extinction for Region A can be calculated from E(B-V) magnitudes given in Ho et al. (1997), but extinction for the other regions B through E are not known.

An extinction model where the extinction increases in proportion with the hydrogen column number density N_{H} may be used for these regions. Using $N_{\text{H}} = 2 \times 10^{21} A_{\text{V}}$ (Schultz & Wiemer (1975), Bohlin et al. (1978), Sneden et al. (1978), Kent et al. (1991)) and $N_{\text{H}} = X_{\text{CO}} I_{\text{CO}}$, the H α extinction A_{R} can be calculated by $A_{\text{R}} = 0.75 A_{\text{V}}$ (Rieke & Lebofsky (1985)). We assume that N_{H} is dominated by molecular hydrogen, because HI and H $_2$ are generally spatially offset in galaxies disks, divided by a transition region. As long as we calculate Σ_{SMD} using only H $_2$, HI should only play a minor role in the extinction, even when calculating global values in Region E. However, this extinction model is known to yield overestimates in regions of higher density (Wong & Blitz 2002), and will give unrealistic values of A_{R} magnitude up to 5 mag. in Region C, 10 mag. in Region B, and even more in Region A. This is clearly an overestimation, because the gas consumption timescale τ derived for these regions using this correction (see section 4.4) will yield τ of only several hundred years, too short to explain the many number of galaxies with such star forming central regions. Therefore, we adopt the same extinction derived in Region A, for Regions B, and C. For Regions D and E, the extinction model explained above is adopted. A source of uncertainty in applying extinction based on molecular density for regions D and E, are the difference in resolution for CO and H α measurements. Light from HII regions is absorbed by dust associated with molecules that are directly between the observer and the HII region in the line of sight. However, the observing beam of the CO observation is far larger than that of the H α observation. Therefore, we can only apply extinction correction based on the average gas density of the region within this CO beam size, whereas the actual extinction of H α light occurs at a smaller scale. This may cause the extinction correction to be an underestimate, but the true correction is impossible unless the H α emitting region is completely resolved in the CO observation. In the case of regions D and E where the beam size is 45 arcseconds, this effect may not be negligible. However, because existing CO observations cannot resolve individual HII regions, we will not further refer to this problem. The effect of neglecting this possible underestimation will be discussed briefly in section 4.2.

Figure 4 is the same as figure 3, with the extinction corrected as explained above. A least squares fit yields $N = 1.33 \pm 0.09$, higher than $N = 1.14 \pm 0.08$ for no extinction correction.

Even with the extinction corrected, however, N is lower than the widely accepted value of 1.4 given by Kennicutt (1998) which includes IR luminous starbursts at dense gas regimes.

Other errors are as follows: H α data used in region D been traced from figure 2 in Rownd & Young (1999), and regions B and C from figure 5 in Koopmann et al. (2001). We assign an error of 0.1 on the ordinate of these data. Other errors are mainly due to difficulty in continuum subtraction. See original paper for details.

4.2. $\Sigma_{\text{SMD}} - \Sigma_{\text{SFR}}$ relation

A least-squares fit to figure 4 results in

$$\log \Sigma_{\text{SFR}} = (1.33 \pm 0.09) \log \Sigma_{\text{SMD}} - 9.95 \pm 0.2,$$

and a best fit to the same data using only region E, or the disk, results in

$$\log \Sigma_{\text{SFR}} = (1.51 \pm 0.6) \log \Sigma_{\text{SMD}} - 10.19 \pm 0.4$$

Similarly, a best fit using only regions A, B, C and D, or the central regions, will yield

$$\log \Sigma_{\text{SFR}} = (1.22 \pm 0.15) \log \Sigma_{\text{SMD}} - 9.68 \pm 0.4$$

The index and the constant of the fits for the disk and central regions are both well within the range of error, although errors for each of the regions are large. This is consistent with the idea that the data plots in the central regions have the same Schmidt law as in the disk regions.

The beam size of the highest density region A (typically 3 arcseconds) corresponds to a projected scale of 250 pc for galaxies in the Virgo cluster. The Schmidt law is thought to be an empirical law which holds at kpc scales within galaxies, but our results imply that smaller scales of several hundred parsecs may still be valid in considering the Schmidt law. It may be noted, that regions close to the nucleus are subject to physical conditions different from the disk. Besides the dense gas tracers such as HCN and CO(J=2-1) observed in these regions, rotation curves in the central kpc are also known to be different from disks, in that rotation becomes nearly rigid compared to nearly flat in the disks (Sofue et al. 2003b). This will lessen the effect of shear which work on the clouds, and may change the efficiency of star formation based on gravitational collapse. These effects could work as systematic change in the relation between gas content and star formation rate in the central regions. However, the index N of the Schmidt law which we have derived from simply fitting figure 4 with a least squares fit indicates no systematic difference in the Schmidt law within the range of error. We conclude that the validity of the Schmidt law at densities from $10^0 \text{M}_{\odot} \text{pc}^{-2}$ up to $10^3 \text{M}_{\odot} \text{pc}^{-2}$ does not change.

It is difficult to consider the Schmidt law for normal galaxies at even higher densities, because doing this will require that we observe with even better spatial resolution; which in turn, will give rise to the problem that we may not be able to observe the molecular cloud and its counterpart star forming region within one beam, as we have seen in section 3 with galaxies at several Mpc from us. As can be understood from this example, the Schmidt law is fundamentally

a correlation seen when averaged over a considerable scale. It may be said that this linear correlation breaks down when averaged over an area of under $\sim 10^2$ pcs. Thus, for higher densities, we must use IR luminous galaxies which have unusually high molecular densities like the studies by Kennicutt (1998). A superposition with these IR luminous starbursts from Kennicutt (1998) and our study is shown in figure 5. Error bars are not shown, but are the same as figure 4. The high density end of normal galaxies exhibit similar Σ_{SMD} and Σ_{SFR} as the lower density end of the starbursts, but the starbursts display higher Σ_{SFR} compared to the Schmidt law derived for normal galaxies at densities above $\Sigma_{\text{SMD}} = 10^3 M_{\odot} \text{pc}^{-2}$. It is important to bear in mind, though, that Σ_{SFR} of the IR starbursts have been derived from IR luminosities, possibly introducing inconsistencies between H α derived rates. Σ_{SFR} derived from H α will indeed give lower Σ_{SFR} if extinction is not corrected. However, we have corrected for H α extinction in our analysis, and Kewley et al. (2002) find that star formation rates derived from extinction corrected H α and FIR luminosities agree well. Therefore, this systematic difference between starbursts and normal galaxies we see in figure 5 may indeed be real, implying that again, we must establish the relation between gas and star formation rates for normal galaxies first in order to gain a fundamental knowledge of the relation between gas content and star formation rate. A least squares fit to the normal and starbursts together, will give $N = 1.41 \pm 0.07$, consistent with the “composite” Schmidt law derived by Kennicutt(1998).

It is justified to say that the derived slope of $N = 1.33$ is relatively reliable, despite the unquantifiable uncertainties, such as X_{CO} , the missing flux problem stated in section 4.1, and the problem of underestimating H α extinction stated in 4.2. This is because allowing for a systematic decrease in X_{CO} by a factor of 3 with galactocentric radius will raise the slope, while on the other hand, correcting for the missing flux and underestimated extinction will increase the density slightly in regions A and B and the star formation rate in regions D and E resulting in the decrease of the slope. These effects will offset to some extent, and changes in the slope will not be so significant. Comparison with Starbursts and normal galaxies will not be affected significantly, because results by Kennicutt(1998) will also have to be corrected in accordance.

4.3. Interpretation of the Schmidt law index N

The widely accepted value of $N = 1.4$ by (Kennicutt 1998) is unchallenged regarding its density range of order ~ 5 , and a simple interpretation of this index is often given that the star formation rate volume density ρ_{SF} scales with gas volume density ρ_{gas} divided by the free-fall timescale of the gas cloud, $t_{\text{ff}} \propto (\sqrt{G\rho_{\text{gas}}})^{-1}$. This will give

$$\rho_{\text{SF}} \propto \frac{\rho_{\text{gas}}}{(\sqrt{G\rho_{\text{gas}}})^{-1}} \propto \rho_{\text{gas}}^{1.5}, \quad (3)$$

which may explain the value of $N = 1.4$. However, this explanation assumes that we are observing a single gas cloud as it gravitationally collapses and eventually forms a star. In actual observations, we are observing an area of the galaxy with a beam in scales of several hundred

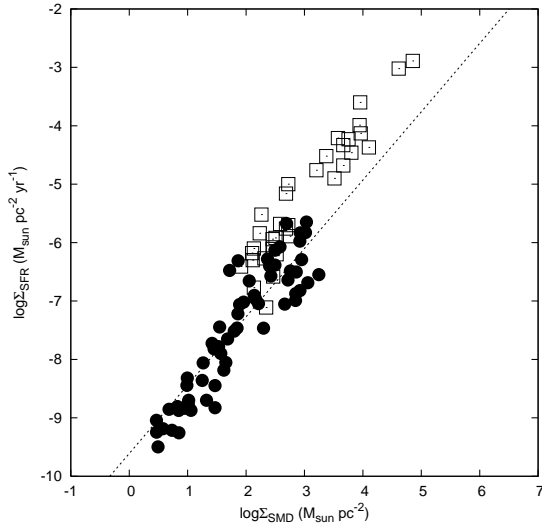


Fig. 5. The composite Schmidt law. Filled circles are the normal galaxies in this study, and open squares are the IR luminous starbursts from Kennicutt (1998). The line is a best fit only to the normal galaxies. Notice that the starbursts are systematically offset from the Schmidt law of normal galaxies in the sense of higher Σ_{SFR} . A best fit for both of the data together will yield $\log \Sigma_{\text{SFR}} = (1.41 \pm 0.07) \log \Sigma_{\text{SMD}} - 9.83 \pm 0.18$

parsecs. Naturally, it is not possible to observe a single cloud, but instead the observer is averaging the gas density and star formation rate of many clouds which are typically several $\times 10$ parsecs in linear scale. In such scales, the increase in the gas density ρ_{gas} (or, Σ_{SMD}) should not be interpreted as an increase in the density of the individual clouds. Instead, we should regard the change as an increase in the number of molecular clouds, within that beam. Therefore, as long as the observing beam is much larger than the typical size of a single molecular cloud, the Σ_{SFR} should increase in proportion with Σ_{SMD} , giving $N = 1$ as the natural result. A best fit to the IR starbursts from Kennicutt (1998) will give $N = 1.28 \pm 0.08$, similar to that for the normal galaxies in our study. However, the factor A of the Schmidt law (provided $\Sigma_{\text{SFR}} = A \Sigma_{\text{SMD}}^N$), determined by the y-axis intercept of figure 5, is higher for these starbursts compared to the normal galaxies, as can be seen clearly from figure 5 with $\log A = -9.09 \pm 0.24$. The datasets for the starbursts have been recalculated using the same X_{CO} as this study. The transition in the Schmidt law from normal galaxies to starbursts seems to be step-like, or that there are two systems in the Schmidt law, with systematically different star formation rates.

4.4. The Star Formation Efficiency

It is convenient to define a star formation efficiency (SFE) by

$$\text{SFE} \text{ (yr}^{-1}\text{)} = \frac{\Sigma_{\text{SFR}}}{\Sigma_{\text{SMD}}}, \quad (4)$$

indicating the efficiency of gas consumption for the formation of stars. Rownd & Young (1999) has shown that SFE is roughly constant within galaxies, using 45 arcsecond resolution data. We show in figure 6 the change in SFE according to the distance from the center, using data

Table 3. The Schmidt Law index

Region	H α extinction correction	N	log A
All	No	1.14 ± 0.08	-9.87 ± 0.20
All	Yes	1.33 ± 0.09	-9.95 ± 0.20
E	Yes	1.51 ± 0.60	-10.19 ± 0.4
A+B+C+D	Yes	1.22 ± 0.15	-9.68 ± 0.4
Kennicutt(1998)	Yes	$1.31 \pm 0.04(1.4 \pm 0.15)$	$-9.45 \pm 0.07(-9.61 \pm 0.13)$
Starbursts	No (IR)	1.28 ± 0.08	-9.09 ± 0.24

The Schmidt Law index and the constant for various regions in our study, and that derived by Kennicutt(1998). A constant value of 1.1 mag. was adopted for H α extinction in Kennicutt(1998). The values for Kennicutt(1998) has been changed to include only molecular gas, whereas the values in parentheses are from the original paper.

in regions A through E. The radii for the plots are taken at the outer edge of each of the regions. Notice that the last panel in figure 6, with all of the galaxies superposed except those excluded in section 3, exhibit a roughly constant SFE of around 10^{-9} to 10^{-10} (yr^{-1}) even in the central regions, with an exception of several galaxies with enhanced SFE. Constant SFE is a manifestation of the Schmidt law with an index $N = 1$, and shows that the gas consumption timescale τ , or the inverse of SFE, is about 1 to 10 Gyr through the entire disk and nucleus for most of the galaxies, and down to 0.1 Gyr for the galaxies with enhanced SFE mentioned above.

5. Conclusions

We have considered the relation between gas content and star formation rate at high molecular densities in the central regions of 23 nearby normal spiral galaxies, using recent high resolution CO observation data and combining it with previous single dish observations. Our main results are as follows;

(1)The Schmidt law, or a simple power law of $\Sigma_{\text{SFR}} \propto \Sigma_{\text{SMD}}^N$, is found to be valid at densities up to $\Sigma_{\text{SMD}} \sim 10^3(\text{M}_{\odot} \text{pc}^{-2})$ for normal spiral galaxies. Regardless of the radical physical differences which these high density regions are subject to, the Schmidt law index is found to be $N = 1.33 \pm 0.09$, with $N \sim 1$ in both central and disk regions.

(2)IR luminous starbursts, which Kennicutt (1998) used to define a composite Schmidt law, is found to display a systematic difference compared to normal galaxies. These starbursts show systematically higher star formation rates compared to that expected from the Schmidt law for normal spirals.

(3)The star formation efficiency (SFE) is found to be roughly constant for more than half of our samples, consistent with the result by Rownd & Young(1999), even in the central few hundred parsecs of spirals. Several other galaxies show higher SFE in the central regions.

Further analysis of the Schmidt law, in order to gain insights in to the physics of star formation depending on local physical states, should involve a galaxy sampled at multiple points within its disk, categorized by its characteristic physical conditions. A fundamental difficulty is that the Schmidt law has a time-averaged nature. Spatial resolution, velocity fields, and the local star formation timescale will alter the relation between gas and star formation tracers. If these uncertainties are removed, we may see sequential differences in the observed Schmidt law according to physical conditions.

Although our results imply that starbursts display a different sequence of gas-star formation rate relation compared to normal spirals, there are still uncertainties in the consistency between Σ_{SFR} derived from IR and H α luminosities which are difficult to quantify. This is because the rate of gas clouds or dust covering a newly born OB star could alter the “true” star formation rate when converted into IR or H α luminosities. In order to compare normal and starburst galaxies in a more quantitative way, it will be important to use a uniform tracer of star formation.

The authors are grateful to T.Handa, for his enlightening comments on the Schmidt law index. H.Nakanishi and S.Onodera were financially supported by a Research Fellowship from the Japan Society for the Promotion of Science for Young Scientists.

References

- Bloemen, J. B. G. M., et al. 1986, A&A, 154, 25
Bohlin, R. C., Savage, B. D., & Drake, J. F. 1978, ApJ, 224, 132
Boissier, S., Prantzos, N., Boselli, A., & Gavazzi, G. 2003, MNRAS, 346, 1215
Cardelli, J. A., Clayton, G. C., & Mathis, J. S. 1989, ApJ, 345, 245
Gao, Y., & Solomon, P. M. 2004, ApJ, 606, 271
Helfer, T. T., Thornley, M. D., Regan, M. W., Wong, T., Sheth, K., Vogel, S. N., Blitz, L., & Bock, D. C.-J. 2003, ApJS, 145, 259
Ho, L. C., Filippenko, A. V., & Sargent, W. L. W. 1997, ApJS, 112, 315
Kennicutt, R. C., & Kent, S. M. 1983, AJ, 88, 1094
Kennicutt, R. C. 1989, ApJ, 344, 685
Kennicutt, R. C. 1998, ApJ, 498, 541
Kent, S. M., Dame, T. M., & Fazio, G. 1991, ApJ, 378, 131
Kewley, L. J., Geller, M. J., Jansen, R. A., & Dopita, M. A. 2002, AJ, 124, 3135
Koopmann, R. A., Kenney, J. D. P., & Young, J. 2001, ApJS, 135, 125
Nakai, N., & Kuno, N. 1995, PASJ, 47, 761
Nishiyama, K., & Nakai, N. 2001, PASJ, 53, 713
Rieke, G. H., & Lebofsky, M. J. 1985, ApJ, 288, 618
Rownd, B. K., & Young, J. S. 1999, AJ, 118, 670
Sakamoto, K., Okumura, S. K., Ishizuki, S., & Scoville, N. Z. 1999, ApJS, 124, 403
Sanders, D. B., Solomon, P. M., & Scoville, N. Z. 1984, ApJ, 276, 182

Schmidt, M. 1959, ApJ, 129, 243
Schultz, G. V., & Wiemer, W. 1975, A&A, 43, 133
Snedden, C., Gehrz, R. D., Hackwell, J. A., York, D. G., & Snow, T. P. 1978, ApJ, 223, 168
Solomon, P. M., Rivolo, A. R., Barrett, J., & Yahil, A. 1987, ApJ, 319, 730
Sofue, Y., Koda, J., Nakanishi, H., Onodera, S., Kohno, K., Tomita, A., & Okumura, S. K. 2003,
PASJ, 55
Sofue, Y., Koda, J., Nakanishi, H., & Onodera, S. 2003, PASJ, 55, 59
Young, J. S., et al. 1995, ApJS, 98, 219
Young, J. S., Allen, L., Kenney, J. D. P., Lesser, A., & Rownd, B. 1996, AJ, 112, 1903
Wong, T., & Blitz, L. 2002, ApJ, 569, 157

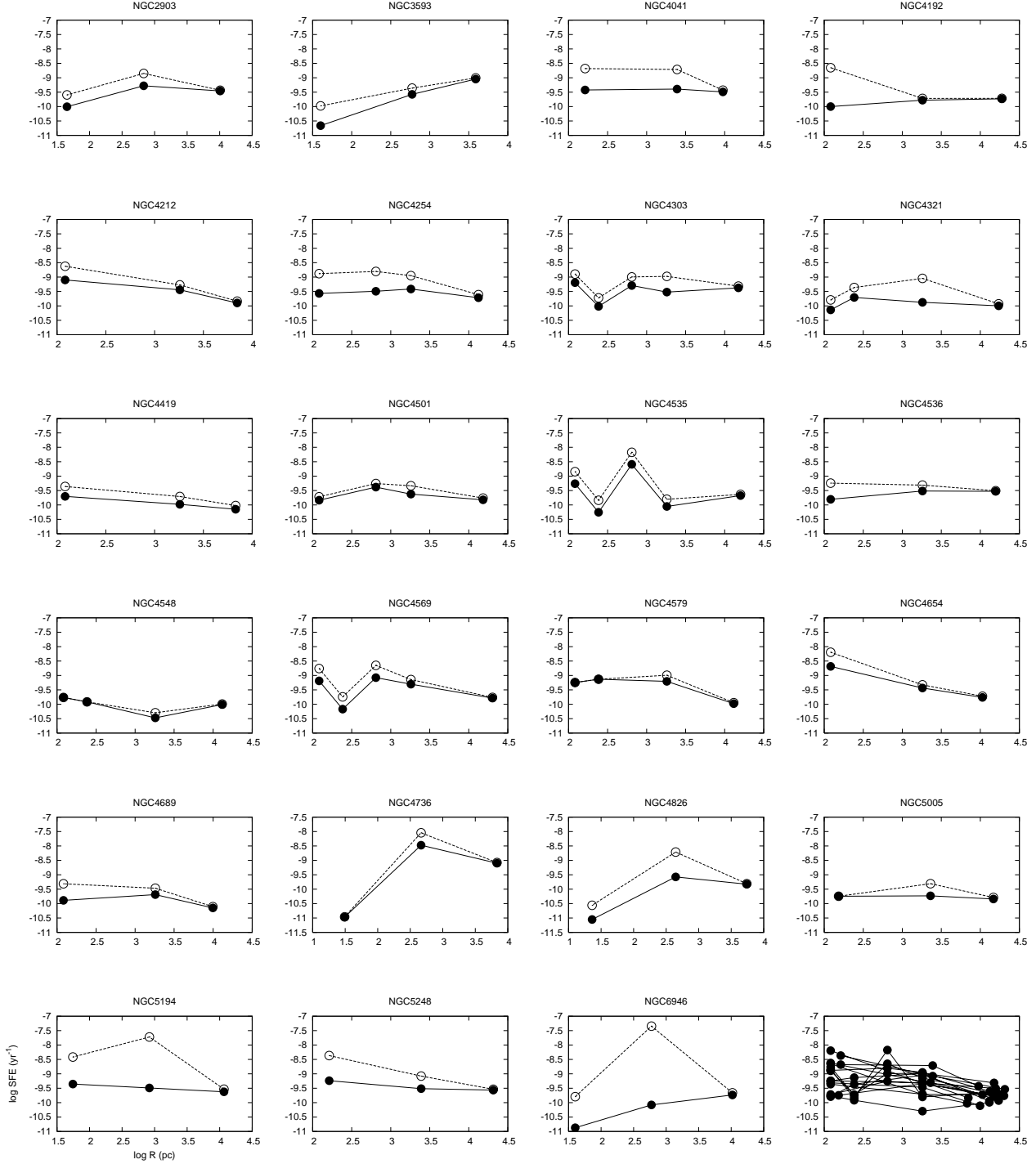


Fig. 6. Star formation efficiency (SFE) vs. galactocentric radius, for all of the sample galaxies. Filled circles are data with no $\text{H}\alpha$ extinction correction, and open circles are extinction corrected data following the method shown in section 4. The bottom right figure is a superposition of the subset of 17 sample galaxies, all corrected for extinction.